Acta Biomaterialia 157 (2023) 124–136

Contents lists available at ScienceDirect

Acta Biomaterialia

journal homepage: www.elsevier.com/locate/actbio

Full length article

Engineered neural tissue made using hydrogels derived from decellularised tissues for the regeneration of peripheral nerves

Simon C. Kellaway[a,b,c,d,*], Victoria Roberton[a,c], Joshua N. Jones[b,d], Rabea Loczenski[b,d], James B. Phillips[a,c,1], Lisa J. White[b,d,1]

[a] Centre for Nerve Engineering, University College London, UK
[b] Division of Regenerative Medicine and Cellular Therapies, School of Pharmacy, Biodiscovery Institute, University of Nottingham, University Park, Nottingham, NG7 2RD, UK
[c] Department of Pharmacology, UCL School of Pharmacy, University College London, 29-39 Brunswick Square, London WC1N 1AX, UK
[d] Biodiscovery Institute, University of Nottingham, University of Nottingham, University Park, Nottingham, NG7 2RD, UK

ARTICLE INFO

Article history:
Received 2 August 2022
Revised 10 November 2022
Accepted 2 December 2022
Available online 7 December 2022

Keywords:
Decellularised ECM
Peripheral nerve regeneration
Peripheral nerve repair

ABSTRACT

Engineered neural tissue (EngNT) promotes *in vivo* axonal regeneration. Decellularised materials (dECM) are complex biologic scaffolds that can improve the cellular environment and also encourage positive tissue remodelling *in vivo*. We hypothesised that we could incorporate a hydrogel derived from a decellularised tissue (dECMh) into EngNT, thereby providing an alternative to the currently used purified collagen I hydrogel for the first time. Decellularisation was carried out on bone (B-ECM), liver (LIV-ECM), and small intestinal (SIS-ECM) tissues and the resultant dECM was biochemically and mechanically characterised. dECMh differed in mechanical and biochemical properties that likely had an effect on Schwann cell behaviour observed in metabolic activity and contraction profiles. Cellular alignment was observed in tethered moulds within the B-ECM and SIS-ECM derived hydrogels only. No difference was observed in dorsal root ganglia (DRG) neurite extension between the dECMh groups and collagen I groups when applied as a coverslip coating, however, when DRG were seeded atop EngNT constructs, only the B-ECM derived EngNT performed similarly to collagen I derived EngNT. B-ECM EngNT further exhibited similar axonal regeneration to collagen I EngNT in a 10 mm gap rat sciatic nerve injury model after 4 weeks. Our results have shown that various dECMh can be utilised to produce EngNT that can promote neurite extension *in vitro* and axonal regeneration *in vivo*.

Statement of significance

Nerve autografts are undesirable due to the sacrifice of a patient's own nerve tissue to repair injuries. Engineered neural tissue (EngNT) is a type of living artificial tissue that has been developed to overcome this. To date, only a collagen hydrogel has been shown to be effective in the production and utilisation of EngNT in animal models. Hydrogels may be made from decellularised extracellular matrix derived from many tissues. In this study we showed that hydrogels from various tissues may be used to create EngNT and one was shown to comparable to the currently used collagen based EngNT in a rat sciatic nerve injry model.

1. Introduction

Peripheral nerve injury (PNI) can be debilitating and, although there have been improvements in microsurgical techniques, clinical outcomes following repair remain poor [1]. For large gaps, in which it is impossible to achieve tension-free end-to-end repair, the current therapeutic gold standard is an autologous transplant, whereby nerve tissue from elsewhere in the patient's body is removed and used to bridge the injury site [1,2]. Autografts contain structural and biochemical cues, in the form of site-appropriate extracellular matrix (ECM) and tissue resident cell populations, providing an environment that is supportive of axonal regeneration

* Corresponding author.
E-mail address: simon.c.kellaway@gmail.com (S.C. Kellaway).
[1] Joint senior authors.

https://doi.org/10.1016/j.actbio.2022.12.003

across the gap. Embracing advances in biomaterials, cell biology, engineering and biomechanics, nerve guidance conduits (NGCs) aim to mimic components of the autograft whilst overcoming the disadvantages of donor site morbidity, morphometric mismatch, the requirement for two surgeries and limitations in availability [3,4]. Desirable features of NGCs include biocompatibility with the surrounding tissue, flexibility, the ability to be sutured into the injury site, and the incorporation of chemotactic, structural, and topographical cues for directional axonal regeneration [3,4]. Tissue derived NGCs have included autologous transplants of skeletal muscle, with its basal lamina and anisotropy, tendon, and vein [5], or rinsed small intestinal segments [6], with each displaying variable abilities to repair peripheral nerve lesions. Decellularised nerve allografts have shown promise in bridging small gap injuries [1,2] and, whilst they contain tissue specific ECM, they lack the necessary cellular support required for regeneration across long gaps [2,7].

Previously we have described a method of producing highly aligned sheets of cells embedded in a purified collagen I matrix, known as engineered neural tissue (EngNT), that can act as a substrate for directional neurite extension *in vitro* and may also be rolled into conduits that promote *in vivo* axonal regeneration [8,9]. To date, we have investigated a variety of cell types including rat derived Schwann cells [9], differentiated adipose-derived stem cells [10] and clinical grade neural stem cells [8,11]. The main material component has remained a purified collagen I hydrogel derived either from rat tail [12] or bovine skin [13].

The ECM exists in a state of dynamic reciprocity with its cellular microenvironment and is intrinsically involved in the maintenance and regeneration of tissues following injury [14]. Decellularised ECM (dECM), derived by removing cellular and antigenic components from mammalian tissues, is biologically complex; it contains structural proteins with naturally occurring motifs for cell adhesion and ligand binding, acts as a reservoir for growth factors, and its degradation products have been shown to promote positive tissue remodelling *in vivo* [14]. It is further possible to partially digest lyophilised dECM powder into a thermoresponsive and pH sensitive hydrogel (denoted dECMh) that can be directly injected to injury sites [15–18] or used as a cell delivery system [19,20].

The use of dECMh for nervous system repair has largely focussed on the central nervous system with injectable hydrogels utilised for traumatic brain injury [21,22] and as cell/ drug carriers for spinal cord repair [23], however recently, considerable research has expanded the use of dECMh for the repair and regeneration of peripheral nerves [24–26]. Within peripheral nerve repair, dECMh have predominantly been used as acellular materials [24,25,27] or to deliver growth factors [26,27]. We hypothesise that due to the high evolutionary conservation of ECM [28] and its innate structural and biochemical cues, dECMh derived from a range of tissues will possess the ability to modulate neural cell behaviour. These materials may therefore provide an environment that improves the conditions of implanted cells within EngNT, subsequently enhancing the neural cell milieu within an injury, and thus enhancing peripheral nerve repair outcomes. Herein we present three dECMh derived from bovine cancellous bone (B-ECM), porcine liver (LIV-ECM) and porcine small intestinal submucosa (SIS-ECM). The resultant hydrogels are required to be predominantly fibrillar in order to accommodate the formation of EngNT via uniaxial tension. Therefore, dECM derived from peripheral nerve was not considered due to its high collagen IV content, thus requiring higher hydrogel concentrations to achieve sufficient gelation [29,30]. B-ECM is 90% collagen I [31]; a B-ECM derived hydrogel has previously shown similar mechanical properties to a collagen I hydrogel [32], and, moreover, some growth factors commonly found in demineralised bone matrix (DBM) can be neurotrophic [33]. Therefore B-ECM was chosen as a candidate for the present study. With respect to B-ECM, similarities in mechanical properties and disparities in biochemical composition led us to investigate LIV-ECM. Nerve conduits fashioned from SIS-ECM have been reported with some promise, although not in hydrogel form [34,35], and so SIS-ECM was selected to be investigated. Each of the dECMh candidate materials were characterised *in vitro* in order to select one candidate to be taken forward into an *in vivo* injury model.

2. Materials and methods

2.1. Bone preparation and decellularisation

Bovine tibias were procured from an EU certified butcher (J. Broomhall Ltd., Dursely, UK). 12–24 month-old animals were slaughtered, and the bones were sliced into 5 mm segments to be shipped on the same day. The segments were stored at -20°C until required. After defrosting to room temperature, the bone was processed to separate the bone marrow and cortical tissue from the cancellous bone. Only the cancellous segments were used and these were washed in phosphate-buffered saline (PBS) containing 0.1% w/v Gentamicin (Invitrogen, Paisley, UK). These segments were then snap frozen in liquid nitrogen and ground into pieces no larger than 4 mm x 4 mm x 4 mm. The pieces were then further submerged in liquid nitrogen and ground into a powder in a commercial coffee grinder (Krups F203).

An adapted version of a previously described method [32] was utilised to remove the mineral content of the cancellous bone granules. The material was suspended in 0.5 N HCl (20 ml/g bone) by agitating using a magnetic stirrer at 300 rpm for 24 hours at room temperature and then rinsed several times in distilled water. The resultant demineralized bone matrix (bDBM) had lipid content extracted via a one hour exposure to a mixture of 1:1 chloroform and methanol (Fisher Scientific, Loughborough, UK) followed by rinsing in methanol and then PBS. The material was then snap frozen in liquid nitrogen, lyophilized for 48 hours and then stored at -20°C.

The lyophilized bDBM was then subjected to an adapted enzymatic decellularization treatment [36]. A solution of 0.05% trypsin (Sigma-Aldrich, Poole, UK) and 0.02% ethylene-diamine tetraacetic acid (EDTA) (Sigma) was used to decellularize the bDBM under constant agitation at 300 rpm at room temperature for 24 hours. This material, now known as bovine decellularized matrix (B-ECM) was agitated in PBS for 24 hours at room temperature to remove any remaining cellular material. The B-ECM was then lyophilized into a powder for 48 hours and then stored at 4°C for later use.

2.2. Liver preparation and decellularisation

Porcine liver was harvested from animals 3-6 months old and procured on the day of slaughter (RB Elliot, Chesterfield, UK). The liver was segmented, connective tissue removed and stored at -20°C for later use. Prior to decellularization, the liver segments were further processed into 3mm slices using a mandolin slicer (Amazing Kitchenware, London, UK).

A previously described method was adapted [37]. The 3mm liver slices were placed in conical flasks and first washed in dH_2O for 15 minutes x three times on a magnetic stirrer at 300 rpm at room temperature. The water was drained, and the slices placed back into the flasks. Three consecutive treatments were then applied: 0.02% trypsin/0.05% EDTA (Sigma) at 37°C, 3% Triton X-100 (Sigma) at room temperature and 4% sodium deoxycholate (Sigma) at room temperature. All treatments were for 1 hour and performed at 300 rpm on a magnetic stirrer and between treatments the slices were gently massaged over a sieve before being washed three times at room temperature in dH_2O at 300 rpm. The resultant LIV-ECM was stored at 4°C in dH2O for 16 hours and weighed.

Depyrogenation was performed using 0.1% peracetic acid in 4% ethanol for 2 hours at room temperature and at 300 rpm on a magnetic stirrer. After sequential washing in PBS and dH_2O, both for 15 minutes, the dECM was snap frozen, lyophilized into a powder and stored at 4°C for later use.

2.3. Small intestinal submucosa preparation and decellularisation

Porcine small intestine was harvested from animals 3-6 months old and procured on the day of slaughter (RB Elliott). A previously described method was adapted to process the small intestine [38]. The jejunum was separated from the large intestine, connective tissue was removed, and it was cut into lengths of approximately 1m. The tissue was washed extensively by running H_2O through the lumen until the runoff became clear, before being sliced longitudinally.

The tissue was then everted luminal side facing up and a portion of the tunica serosa removed through gentle abrasion. The tissue segment was then inverted to be abluminal side facing up and the muscular externis removed via mechanical abrasion; a motion that further removes the tunica serosa underneath. The resultant submucosa was washed in PBS on a mechanical shaker at 300 rpm at room temperature. Subsequently, the SIS was treated with 0.1% peracetic acid in 4% ethanol for 2 hours followed by two sequential washes in PBS and deionised water; all treatments performed on a mechanical shaker at 300 rpm at room temperature. The resultant SIS-ECM sheets were then frozen at -80°C for 24 hours, lyophilised and stored at 4°C. Sheets were milled into powder before digestion.

2.4. ECM hydrogel formation

2.4.1. Digestion and solubilisation

A previously described method was employed to achieve dECM solubilisation [32]. Lyophilised dECM powders were added to 1 mg/ml pepsin in 0.01 N HCl solution to make up a final dECM concentration of 10 mg/ml. In other words, 1 g dry dECM was mixed with 100 mg pepsin in 100 ml 0.01 N HCl. The suspension was mixed on a magnetic stirrer at room temperature for 48 hours (LIV-ECM, SIS-ECM) or 72 hours (B-ECM) until no visible particulate was observed. Now known as an “ECM digest” these were subsequently centrifuged at 2000 rpm for 5 minutes, aliquoted and stored at - 20°C or used immediately.

2.4.2. Neutralisation and gel formation

Gelation was achieved via basic neutralisation as previously described [32]. All solutions were kept at 4°C. Briefly, ECM digests were mixed with 0.1 N NaOH (1/10 volume of pre-gel solution) and 10X PBS (1/9 volume of pre-gel solution). 1X PBS was further used to adjust the solution to the desired concentration and volume before raising the temperature to 37°C to promote gelation. Previous work showed that 2 mg/ml collagen I hydrogels showed optimal contraction and alignment [39], however, at this concentration dECMh were not able to form a robust hydrogel. As such, the experiments in this work used 4 or 6 mg/ml dECMh.

2.5. dECM characterisation

2.5.1. Histology

Tissue was fixed in 3.7% (w/v) paraformaldehyde (PFA), using a 20:1 ratio (PFA:Tissue), straight after each experiment. The tissue was incubated in PFA for 48 hours before rinsing with the same volume PBS. An automated tissue processor (Leica TP1020) was used to penetrate the tissue with melted paraffin wax. Briefly, the tissue was dehydrated using increasing concentrations of ethanol (25%; 50%;75%; 95%; 100%) to fully remove water content from the tissue. Once the tissue was fully penetrated by ethanol, the ethanol was replaced by Histoclear, a clearing agent that is miscible in ethanol and paraffin wax. In the final step, Histoclear was replaced with melted paraffin wax (~60°C). Following this process, the tissue was wax embedded using a wax embedder (Leica EG1160). Briefly, the tissue was placed in a stainless-steel base mould, orientated as required and then covered with melted wax before left to set on a cooled plate (-20°C) until fully hardened. The histopathology unit at Queens Medical Centre (QMC) Nottingham (UK) conducted sectioning, staining and imaging. Tissue sections were cut into 5 mm sections. Three sections were taken per sample. A Hamamatsu Nanozoomer NDP slide scanner was used to scan all slides.

The following stains were chosen for histological analysis: Haematoxylin & Eosin (nuclei and cytoplasm), Alcian blue (glycosaminoglycans), and picrosirius red (collagen).

2.5.2. dsDNA quantification

An adaptation of a previously reported method was used to quantitatively measure double stranded DNA (dsDNA) content [40]. ECM powders of known weight were digested in a proteinase k solution containing 0.5M EDTA, 10% Sodium dodecyl sulphate (SDS), 5M Sodium chloride (NaCl) for 24 hours at 60°C. DNA was extracted from the proteinase k digests by addition of 25:24:1 (v/v/v) phenol/ chloroform/ isoamyl alcohol. A DNA pellet was formed through precipitation at -80°C from the aqueous phase via addition of 3 M sodium acetate (pH 5.2) and 100% ethanol followed by centrifugation at 10,000 g for 10 minutes. Pellets were washed in ethanol, dried, and then resuspended in 1 x TE buffer (PanReac AppliChem, Italy). Total dsDNA concentration was calculated using a Quant-iT^{TM} PicoGreen dsDNA assay kit (Invitrogen, Paisley, UK). Standard curves of 0 to 1000 ng/ml were produced and the DNA extracts were diluted and absorbances read using a plate reader (Tecan Infinite 200. Tecan, Reading, UK).

2.5.3. Glycosaminoglycan quantifications

DMMB reagent, a light-sensitive cationic dye that specifically binds to sulphated glycosaminoglycans (sGAG), was produced via dissolving 16 mg/L of 1,9-dimethylmethylene blue in 5 mL of 100% ethanol and addition of 40 mM glycine 40 mM NaCl. The pH of the DMMB solution was adjusted to 1.5 pH using HCl.

ECM powders of known weight were digested in 0.125 mg/ml papain in phosphate buffer supplemented with 0.01 M cysteine and 0.01 M EDTA at 60°C for 24 hours. The digests were then diluted and placed in a 96 well-plate before adding DMMB solution. A standard curve was produced of 0 -75 µg/ml chondroitin sulphate from shark cartilage and absorbance was measured at 540 nm with a reference of 620 nm using a Tecan 200 plate reader.

2.5.4. Rheological characterisation of dECM hydrogels

Rheological measurements were carried out using a Physica MCR 301 rheometer. The apparatus was cooled in a humidified chamber to 4°C prior to digest addition and then warmed to 37°C to induce gelation. 200 µl of ECM digest was added to the lower parallel plate, cooled to 4°C; there was a 0.2 mm gap between the two 25 mm parallel plates. A time sweep of 20 minutes at constant angular frequency (1 rad/s) and amplitude (1% oscillatory strain) with readings every 30 s was first performed to record gelation kinetics. The gel was then subjected to an amplitude sweep from 0.1% to 200% oscillatory strain with a constant angular frequency of 1 rad/s to record strain stiffening behaviour and maximum moduli.

2.6. Cell culture

2.6.1. F7 Schwann cell culture

SCL4.1/F7 (Health Protection Agency, UK) Schwann cells were maintained in culture medium (Dulbecco’s modified eagle’s

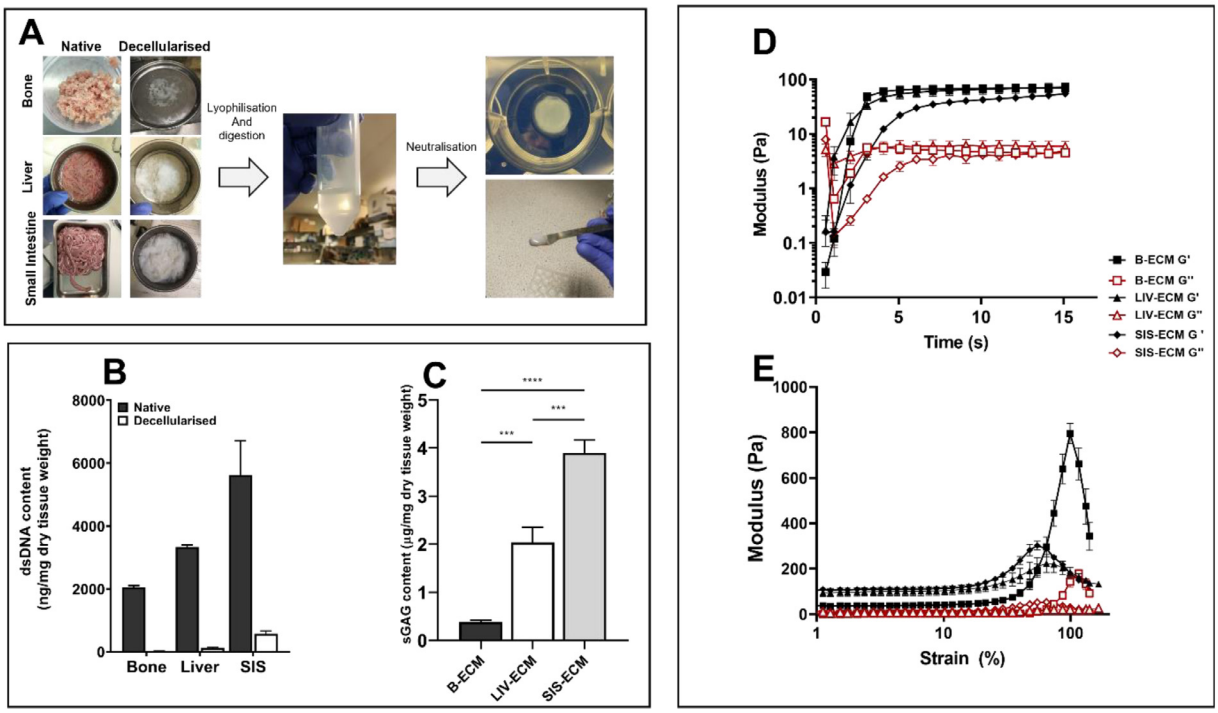

Fig. 1. dECM and dECM hydrogel production with biochemical and rheological analysis. [A] Decellularisation of tissues, pre-gel production via pepsin digestion and neutralisation to pH 7.4 form hydrogels under physiological conditions. [B-C] Biochemical analysis: dsDNA content of native and decellularised tissues to confirm decellularisation [B] with sGAG quantification of dECM [C]. [D-E] Rheological analysis: Time sweep of 4 mg/ml dECM hydrogels to observe gelation profile [D] and strain sweep of 4 mg/ml dECM hydrogels to observe material response to strain [E]. Data are mean ± SEM, n = 4 [B-C], n = 3 [D-E]. One-way ANOVA with Tukey's multiple comparisons test. Statistical significance is designated as ns = not significant, $^{**}P < 0.01$, $^{***}P < 0.001$, $^{****}P < 0.0001$.

medium (DMEM), Sigma) supplemented with penicillin (100 U/ml)/ streptomycin (100 mg/ml) (Sigma) and 10% v/v foetal bovine serum (Thermo Fisher Scientific) in standard cell culture flasks.

2.6.2. Dorsal root ganglia preparation and culture

All experimental procedures involving animals were conducted in accordance with the UK animals (Scientific Procedures) Act (1986) and approved by the UCL animal ethics advisory group. Dissected dorsal root ganglia (DRGs) were prepared from adult (200-300g) Sprague Dawley rats, the spinal nerve, ventral and dorsal roots removed before incubation in 0.125% collagenase (Sigma) for 1.5 hours at 37°C. Dissociation was aided by trituration followed by two washes in cell culture medium (DMEM). The suspension was plated onto cell culture flasks coated with poly-d-lysine (Sigma) (PDL) and incubated for 24 hours with cytosine arabinoside (0.01 mM) to deplete satellite glia.

2.6.3. Cellular hydrogel production

dECM digests were neutralised and made up to desired concentrations and volumes using a buffer solution containing 0.1 N NaOH (Sigma), 10X MEM (Thermo Fisher Scientific) and 1X PBS (Sigma). Following neutralisation, cell laden pre-gels were prepared by using 90% v/v dECMh (4 or 6 mg/ml) with 10% v/v F7 cell suspensions with the correct cell number to achieve the desired final density. Gelation was then induced by incubation at 37°C for 45 minutes. 75 µl gels were prepared for the 96-well plate contraction assay, whereas 400 µl gels were prepared and placed in tethering moulds in 6-well plates to create aligned anisotropic engineered neural tissue (EngNT). Tethering moulds were made from polyether ether ketone and consisted of a rectangular chamber 15 × 3 × 6 mm with two vertical posts at each end (Fig. 1B) [41]. For the contraction assay the gels were mechanically removed from the edge of the well plate and 200 µl of DMEM added to each well to form "free-floating" cellular gels. For the alignment assay, following gelation in the tethered moulds enough DMEM was added to each 6-well plate to cover the entire mould. All gels were further incubated at 37°C in a humidified incubator with 5% CO_2/ 95% air for 24 hours.

2.6.4. EngNT sheet production

Plastic compression was performed by removing the hydrated cellular gels from their 400 µl moulds and placing them underneath raft absorbers, separated by a fabric mesh for 15 seconds (SIS-ECM), 25 seconds (B-ECM), 45 seconds (LIV-ECM), and 3 minutes (Collagen I); different times associated with different EngNT structural integrity. The resultant sheets of EngNT were then either placed in media for co-culture with neurons or fixed in 4% paraformaldehyde overnight at 4°C for immunostaining.

2.7. Cell assays

2.7.1. 3D CellTiter-Glo®

dECM and collagen I (Collagen Solutions, UK) hydrogels at concentrations of 6 mg/ ml were formed, seeded with F7 Schwann cells at a concentration of 0.5 × 10^6 cells/ ml, and placed in a cell culture incubator at 37°C and 5% CO_2/ 95% air for 1 hour. DMEM was aspirated and the gels placed in a black 96-well plate. 1:1 DMEM: CellTiter-Glo® reagent was added and the plate placed on a shaker at 120 rpm for 20 min. Luminescence was measured using a microplate reader.

2.7.2. Neurite outgrowth assay

Neurons obtained from DRG cultures were seeded on top of 19 mm cover slips coated with 50 µg/ml poly-d-lysine (PDL; Sigma-Aldrich) followed by either 50 µg/ml collagen I or 50 µg/ml dECM. Cultures were covered in DMEM-complete and maintained at 37°C in a humidified incubator with 5% CO_2/ 95% air for 72

hours, following which they were washed in PBS and fixed in 4% paraformaldehyde overnight at 4°C for immunostaining.

2.7.3. Neurite co-culture assay

Dissociated DRGs were seeded on top of EngNT sheets in 6-well plates (around 2 DRGs per construct), allowed to settle for 30 minutes before addition of enough DMEM-complete to completely cover the constructs and incubated at 37°C in a humidified incubator with 5% CO_2/ 95% air for 72 hours. Following incubation, the constructs were washed with PBS and fixed in 4% paraformaldehyde overnight at 4°C for immunostaining.

2.8. Repair of 10-mm sciatic nerve defect

All experimental procedures involving animals were conducted in accordance with the UK animals (Scientific Procedures) Act (1986) and approved by the UCL animal ethics advisory group. Female Wistar rats (200-225 g) were used for the following experiments due to their decreased growth rate, when compared to males.

The left sciatic nerves of each rat were transected at mid-thigh level to form a 10 mm gap. 12 mm silicone tubes were introduced into the injury site either as empty tubes or filled with 400 µl EngNT derived from purified rat tail collagen I or B-ECM hydrogels. 1 mm of the distal and proximal nerve stumps were inserted into corresponding ends of the devices and sutured in place with epineural sutures (Ethilon 10/0: Ethilon-Johnson & Johnson, Brussels, Belgium). The muscular layer was closed with sutures (Ethilon 4/0) and the wounds closed with wound clips. Animals were monitored for 28 days post-surgery.

Following the 28-day experimental period, animals were culled via overdose of anaesthesia. Sciatic nerves were harvested under a dissecting microscope: connective tissue around the conduits was separated from the muscle and the nerves cut approximately 6 mm from the distal and proximal sutures (Supplementary Fig. 4). Nerves were immediately placed in 4% paraformaldehyde on ice and fixed overnight at 4°C. The silicone tubes were then removed, and the nerves were then placed in 15% sucrose in PBS overnight, or until sunk, before being placed in 30% sucrose overnight. The nerves were then dissected as depicted in Supplementary Fig. 5 and embedded in 1:1 v/v sucrose in PBS: optimal cutting temperature (OCT; Leica) solution within a cryosection mould (TAAB). Moulds were placed in liquid nitrogen to snap-freeze the samples that were then stored at -20°C for sectioning.

2.9. Image analysis

2.9.1. Measurement of contraction

Following their 24-hour incubation time, images were captured of each gel following removal of culture media. Percentage contraction was calculated in ImageJ by measuring the area of each gel as a percentage of the total area of the well.

2.9.2. Quantification of cellular alignment

Z-stacks of cellular constructs were imaged from specified regions of the gel and imported into Volocity™ (Perkin Elmer, UK) for 3D image analysis. The software was used to assign each cell as an "object" with parameters applied to separate touching objects and to exclude objects outside a designated size range. Each object was then assigned a length corresponding to their longest axis, and the software was then used to calculate their angle of deviation from the longitudinal axis of the construct.

2.9.3. Measurement of neurite length in vitro

Neurite length was automatically calculated using the "Simple Neurite Tracer" plugin in ImageJ. 3 whole gels/ coverslips per condition were used for data collection. Mean neurite length was calculated as the mean length of neurites within each field, whilst longest neurite was calculated as the longest neurite extending from each DRG neuron.

2.9.4. Automatic counting of neurofilament positive axons from in vivo *experiments*

Tile scan confocal images were obtained from a Zeiss LSM710 confocal microscope. These were used to quantify the number of neurofilament positive axons present in each region of the graft following surgical nerve repair. Volocity™ software was used to automate this process. Briefly, the endoneurium was selected as the region of interest and the image cropped. This was followed by the assignment of objects of a minimum threshold of intensity, corresponding to axons, as well as size exclusion of objects and separation of touching objects. Three areas on each section were randomly selected for manual counting to compare with the automated protocol to ensure accuracy. The protocol was accepted if the two separate counts fell within 10% range.

2.9.5. Blood vessel counting and lumen diameter measurement

A Zeiss AxioLab.A1 fluorescence microscope was used to count RECA-1 positive blood vessels. Blood vessels were only counted if they contained a clear lumen. Measurement of blood vessel diameter was conducted on fluorescence images using ImageJ.

2.10. Statistical analysis

Normality tests were conducted to assess distribution of data. One-way or two-way analysis of variance (ANOVA) tests were followed by a Tukey test (with Kramer correction for unequal sample sizes, as noted). For all tests, $^{*}P < 0.05$, $^{**}P < 0.01$, $^{***}P < 0.001$, and $^{****}P < 0.0001$ were considered to be significant. All data are expressed as mean ± SEM.

3. Results

3.1. Biochemical characterisation of dECM powders

Following decellularisation treatments the resultant tissues appeared white or translucent (Fig. 1A). Decellularisation was confirmed via a lack of observable nuclei in H&E staining (Supplementary Fig. 1) and over 90% reductions in dsDNA content (Fig. 1B). sGAG were further present in all dECM materials (Fig. 1C), however B-ECM presented the lowest sGAG content with 0.380 ± 0.04 µg/ mg dry tissue weight, whereas the SIS-ECM possessed the highest with 3.90 ± 0.27 µg/ mg. Picosirius red staining revealed an abundance of collagenous fibrils throughout all three dECM scaffolds (Supplementary Fig. 1) and the maintenance of both the LIV-ECM and SIS-ECM native collagen architecture. The Alcian blue staining shows a strong retention of sGAG within the SIS-ECM and some retention within the LIV-ECM when compared with their native staining.

3.2. Rheological characterisation of dECM hydrogels

Robust hydrogels were formed from all three dECM materials (Fig. 1A). A sigmoidal gelation profile was observed for each of the hydrogels (Fig. 1D). B-ECM hydrogel had the highest complex modulus of 17.57 ± 0.69 Pa, followed by the LIV-ECM hydrogel (13.25 ± 1.90 Pa), whilst the SIS-ECM hydrogels had the lowest complex modulus of 11.45 ± 1.6 Pa. Every material began to stiffen at around 25% strain (Fig. 1E); however, the SIS-ECM hydrogel reached its maximum modulus at 47.6% strain, in contrast to the B-ECM and LIV-ECM hydrogels maximum moduli occurring at 99.5% and 73.9% strain respectively. The B-ECM hydrogel had the

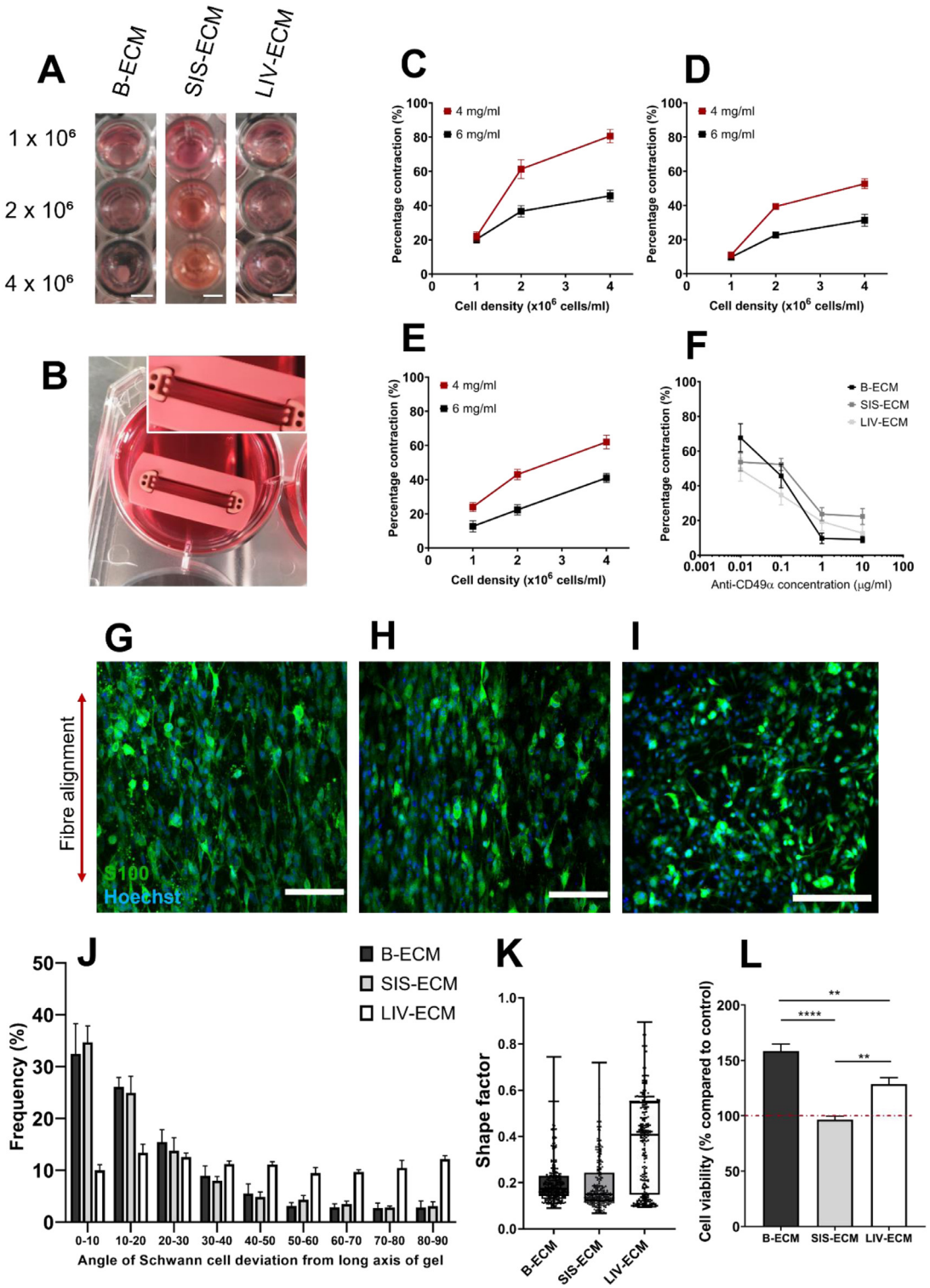

Fig. 2. F7 Schwann cell response to dECM hydrogels. [A] Free-floating dECM hydrogels containing different seeding densities of F7 Schwann cells following a 24-hour incubation time, scale bars = 2 mm. [B] 4 mg/ml dECM hydrogel seeded with 4 × 10^6 F7 Schwann cells inside a tethered mould. [C-E] Contraction profiles for B-ECM [C], SIS-ECM [D], and LIV-ECM [E] 4 mg/ml and 6 mg/ml hydrogels at different seeding densities, mean ± SEM, N = 3 from 3 independent experimental gel digest batches. Contraction is displayed as a percentage and calculated via comparing the area of the top of the gel to the area of the well. [F] Contraction profile of 4 mg/ml dECM hydrogels seeded with 4 × 10^6 F7 Schwann cells and different concentrations of anti-CD49α to block integrin α1. [G-I] Confocal micrographs of F7 Schwann cells seeded at 4 × 10^6 in B-ECM [G], SIS-ECM [H], and LIV-ECM [I] 4 mg/ml hydrogels, scale bars = 100 μm. [J] Angle of Schwann cell deviation from long axis of cellular constructs [K]. Shape factor analysis for F7 Schwann cells within dECM hydrogels. [L] Metabolic activity of F7 Schwann cells seeded at 0.5 × 10^6 in 6 mg/ml dECM hydrogels as a percentage to collagen controls (red dotted line). Data are mean ± SEM, n = 5 gels per condition from 3 independent experimental gel digest batches. One-way ANOVA with Tukey's multiple comparisons test. Statistical significance is designated as ns = not significant, $^{**}P < 0.01$, $^{***}P < 0.001$, $^{****}P < 0.0001$.

largest strain stiffening response, followed by SIS-ECM, whilst LIV-ECM had the lowest. Data for 8 and 6 mg/ml hydrogels are shown in Supplementary Fig. 2.

3.3. F7 Schwann cell mediated contraction in dECM hydrogels

Following a 24-hour incubation, 4 and 6 mg/ml hydrogels seeded with F7 Schwann cells were seen to have contracted away from the edges of 96 well-plates (Fig. 2A) and tethering moulds (Fig. 2B). dECM hydrogel contraction was dependent on both dECM and cell seeding concentrations (Fig. 2C-E). Contraction was highest for 4 mg/ml B-ECM hydrogels seeded with 4×10^6 cells/ml (80.7 ± 6.8%) and lowest for the 6 mg/ml LIV-ECM hydrogels seeded with 0.5×10^6 cells/ml (11.0 ± 2.2%). When further incubated with anti-CD49α to disrupt $\boldsymbol{\alpha}$1 integrin-mediated cell-matrix interaction, F7 Schwann cell-seeded 4 mg/ml dECM hydrogel contraction was inhibited in a dose-dependent manner (Fig. 2F). Integrin blocking was most effective for the B-ECM hydrogels, reducing contraction from 67.7 ± 8.1% to 9.0 ± 1.7%. Contraction was reduced from 49.3 ± 6.7% to 12.7 ± 4.7% and 53.7 ± 5.1% to 22.3 ± 4.5% in LIV-ECM and SIS-ECM hydrogels respectively.

3.4. dECM hydrogels support F7 Schwann cell alignment

Fig. 2G-I shows that the magnitude of cellular self-alignment of F7 Schwann cells differed between the dECM hydrogels following a 24-hour incubation. F7 Schwann cells within B-ECM and SIS-ECM hydrogels appeared to show a higher level of alignment with respect to their LIV-ECM derived counterpart and this was supported via the measurement of the angle of deviation of single cells from the long axis of the gel constructs (Fig. 2J). F7 Schwann cells further presented an elongated, bipolar morphology within B-ECM and SIS-ECM hydrogels (Fig. 2G &H) and appeared more rounded within the LIV-ECM hydrogels (Fig. 2I); this was confirmed through shape factor analysis of individual cells (Fig. 2K). The metabolic activity of the F7 Schwann cells was highest for B-ECM gels and lowest for the SIS-ECM gels, respectively 158.9 ± 6.2% and 96.5 ± 3.2% of the collagen control. Within the LIV-ECM, the F7 Schwann cells were observed to have 128.7 ± 5.8% metabolic activity of the collagen control (Fig. 2L).

3.5. dECM coated coverslips support DRG neurite outgrowth

dECM coatings were applied to coverslips to investigate interactions between the biochemical components of the different dECM on primary neuronal cell cultures. DRG neurite extension was observed on each of the dECM coatings as well as on the collagen I comparator (Fig. 3A-D). No significant difference was found between the groups for either mean neurite length (Fig. 3E) or longest neurite lengths (Fig. 3F). Mean neurite lengths for B-ECM and collagen I coatings were both found to be 108.9 ± 10.7 µm and 101.3 ± 9.0 µm, respectively, whilst LIV-ECM and SIS-ECM coatings were 93.1 ± 8.3 µm and 94.0 ± 2.8 µm, respectively.

3.6. dECM EngNT support DRG neurite outgrowth

Primary DRG cultures were further cultured onto EngNT sheets made using dECM or collagen I to investigate neurite extension as a function of ECM components within a 3D *in vitro* model. Following stabilisation, the EngNT derived from SIS-ECM hydrogels appeared to lose its structural integrity in comparison to the other materials (Supplementary Fig. 3). All types of EngNT supported neurite outgrowth (Fig. 3G-J). B-ECM EngNT had the highest mean neurite length of 170.7 ± 6.6 µm, equivalent to 170.3 ± 3.5 µm observed on the collagen I derived EngNT (Fig. 3K). Mean neurite lengths on LIV-ECM and SIS-ECM EngNT however were significantly lower: 114.1 ± 3.1 µm and 107.5 ± 6.6 µm, respectively ($P <$ 0.001). Whilst neurites extending on B-ECM, SIS-ECM and collagen I derived EngNT (Fig. 3G, H, & J) were seen to align along the long axis of the gel, those on the LIV-ECM derived EngNT extended in a non-directional manner (Fig. 3I).

3.7. B-ECM EngNT promotes similar axonal regeneration to collagen I derived EngNT in vivo

At 28 days post transplantation in a rat sciatic nerve injury model, tissue regeneration across the 10 mm gaps varied between the groups. When compared with the empty silicone tube, a more robust tissue can be observed to bridge the proximal and distal stumps of both EngNT groups, however the tissue was not as substantial as that seen in the autograft (Supplementary Fig. 5). Histological analysis of the proximal sections (Supplementary Fig. 4) showed that, in all groups, nerve tissue densely populated with axons had infiltrated the conduits and grafts (Fig. 4A). Quantitative analysis showed that the autograft and EngNT groups showed similar axon counts at the proximal region of the graft whilst slightly lower axon counts were observed in the empty tube (Fig. 4B). The distal region counts show more variation with 85.8 ± 68.0 axons seen in the distal region of the empty tube group compared to the 6098.7 ± 660.0 axons in the autograft group. 2461.2 ± 1082.9 axons were observed at the distal region of the B-ECM EngNT group whilst 1966.7 ± 402 axons were counted in the collagen I derived EngNT group. Fig. 4C shows that axonal regeneration was similar between the B-ECM EngNT and collagen I EngNT groups (32.4 ± 12.8% and 28.1 ± 6.5% of the proximal region, respectively). This was significantly ($P < 0.0001$) higher than that observed in the empty silicone tube control (1.4 ± 1.1% of the proximal region). The autograft, however, showed 75.2 ± 6.4% axonal regeneration.

S100 and neurofilament staining within the empty tube revealed small, yet organised areas of tissue (Fig. 5). Neurofilament positive axons and S100 positive cells may be seen across the longitudinal sections of the B-ECM EngNT and collagen I derived EngNT groups. In both groups the axons and Schwann cells appear more ordered at the proximal regions when compared to the distal. In comparison, the autograft group showed a sparser organisation of Schwann cells, although this structure was largely maintained throughout toward the distal end (Fig. 5).

Fig. 6 shows that the autograft group had the highest blood vessel counts at both the proximal (55.2 ± 4.8) and distal (55.1 ± 8.6) sections. In contrast the empty tube, B-ECM EngNT, and collagen I derived EngNT all possessed similar blood vessel counts of 40.4 ± 2.4, 43.3 ± 4.1, and 39.0 ± 6.7 at the proximal region, respectively and 37.0 ± 2.0, 37.9 ± 4.3, and 38.1 ± 3.8 at the distal region of the graft, respectively. Blood vessel diameters appeared consistent within all groups at around 10 µm at the distal and proximal regions.

4. Discussion

Previously described EngNT utilised a purified collagen I hydrogel as a biomaterial for the delivery of a variety of cell types for peripheral nerve repair [8,9,11]. Here we present three alternative biomaterials in the form of dECMh derived from a range of different tissues. dECM are complex biomaterials that can improve the regenerative potential of cell therapies via the presentation of structural and biochemical cues that are more representative of those observed *in vivo* [14,42].

The three dECM materials were biochemically distinct. Lower dsDNA contents, whilst indicative of a more complete decellularisation process, were associated with a lower sGAG content. Achieving sufficient removal of antigenic material whilst retaining biologically active soluble factors is important when considering the effect dECM materials have *in vitro* and *in vivo*. In particular

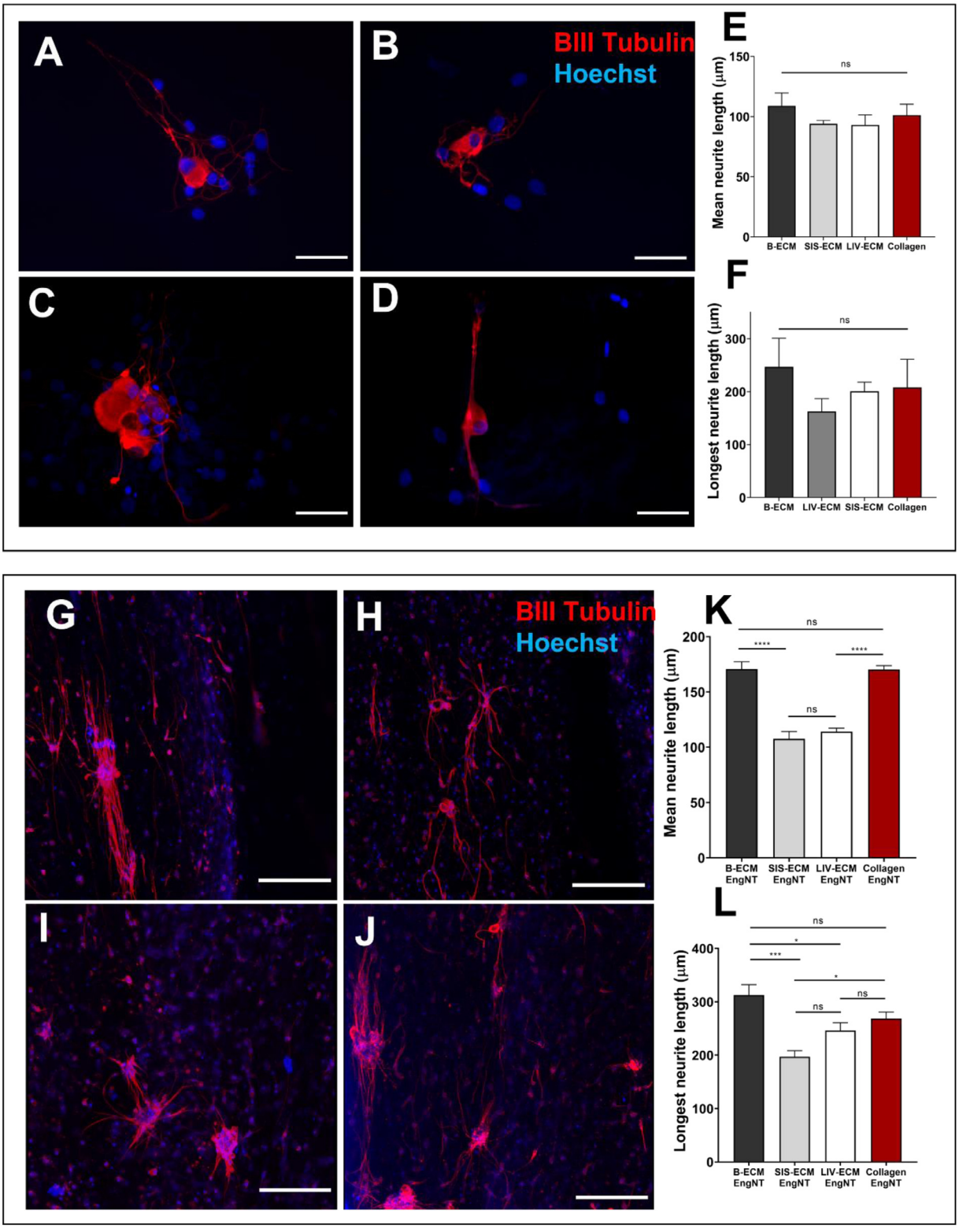

Fig. 3. Dorsal root ganglia response to dECM and dECM EngNT. Rat DRGs after 48 hour incubation seeded on coverslips coated with 50 µg/ml B-ECM [A], SIS-ECM [B], LIV-ECM [C], and collagen I [D]. Scale bars = 100 µm. Mean neurite length [E] and longest neurite length [F] for DRGs seeded on dECM and collagen I coated coverslips. 3D co-cultures of DRGs seeded on B-ECM [G], SIS-ECM [H], LIV-ECM [I], and collagen I [J] derived EngNT. Scale bars = 200 µm. Mean neurite length [K] and longest neurite length [L] for 3D co-culture models. Data are presented as means ± SEM, N = 3 (coverslips) N = 5 (co-culture). One-way ANOVA with Tukey's post hoc test, $^{*}P < 0.05$, $^{***}P < 0.001$, $^{****}P < 0.0001$.

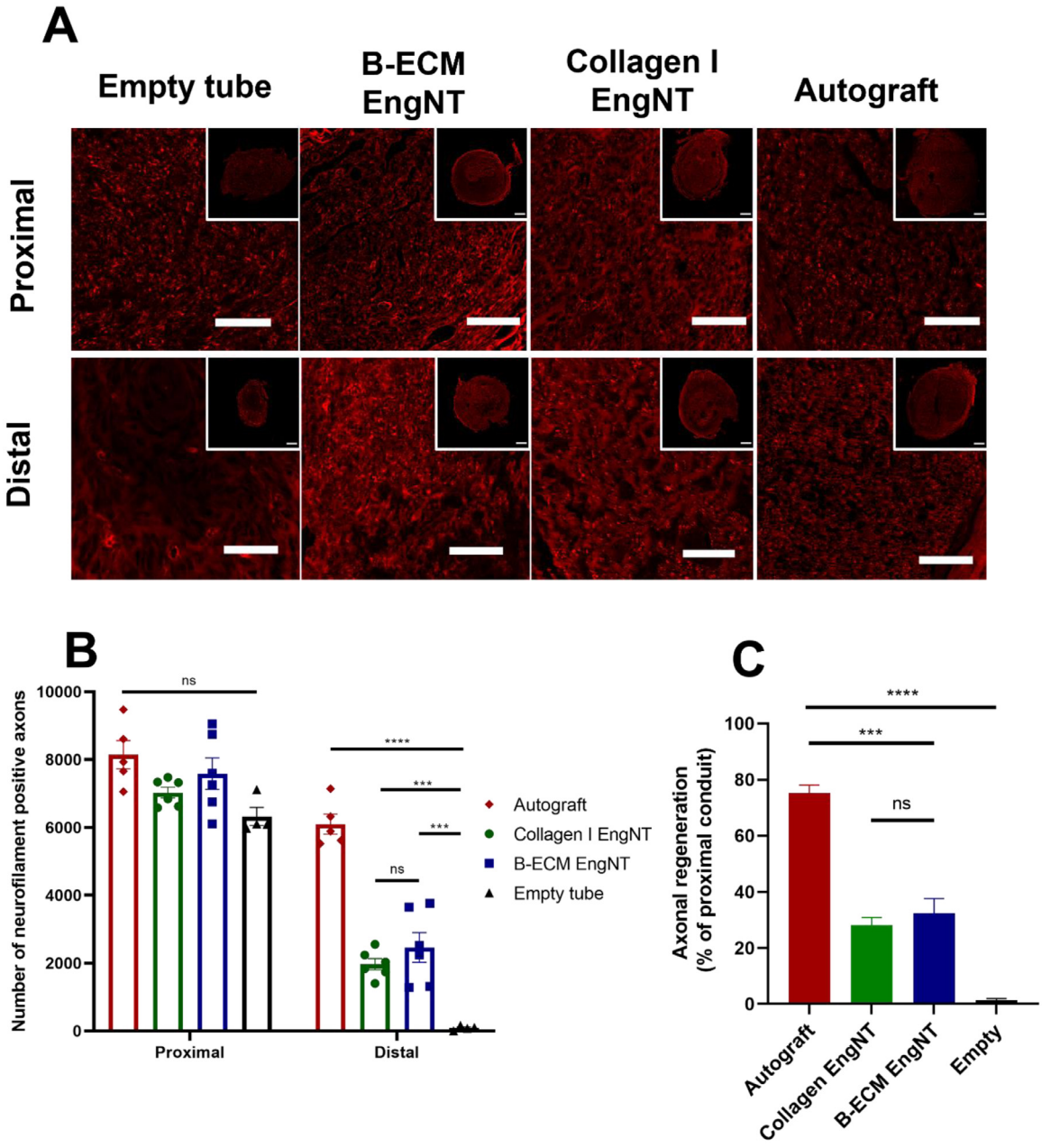

Fig. 4. B-ECM EngNT promotes similar axonal regeneration to collagen I EngNT *in vivo*. Representative confocal micrographs of neurofilament positive axons in the proximal and distal regions of empty tubes, collagen I EngNT, B-ECM EngNT, and autografts 28 days post-surgery. Scale bars = 100 μm [A]. Axon counts for the proximal and distal location of each group via the quantification of neurofilament positive axons in each region [B]. Percentage of axons in distal graft compared to proximal graft [C]. Data are mean ± SEM N = 6 animals for the B-ECM and collagen EngNT, N = 5 animals for the autograft, and N = 4 animals for the empty tube. Two-way ANOVA with Tukey's multiple comparisons test (with Kramer correction for unequal sample sizes) [A]. One-way ANOVA with Tukey's multiple comparisons test (with Kramer correction for unequal sample sizes) [B]. Statistical significance is designated as ns = not significant, $^{**}P < 0.01$, $^{***}P < 0.001$, $^{****}P < 0.0001$.

for xenogeneic dECM, residual cellular material such as dsDNA or lipids can cause adverse inflammatory responses [43], whereas removal of soluble components such as growth factors and sGAG can significantly impair the bioactivity of the scaffolds [44,45]. Additionally, some harsh decellularisation treatments that achieve high cellular removal have the potential to cause irreversible structural damage to the ECM components and so it cannot be assumed that a more decellularised tissue is inherently superior to a less decellularised tissue [46,47]. There was a higher metabolic activity of F7 Schwann cells in the B-ECM, which had a lower dsDNA content whereas there was lower metabolic activity in the SIS-ECM which had a higher dsDNA content. This may be due to a greater level of cellular survival within the B-CM hydrogel.

Sigmoidal gelation curves were observed unsurprisingly, due to these dECM primarily being collagen based and this behaviour has been shown before in B-ECM derived hydrogels [32]. However, the strain stiffening responses differed greatly, likely due to their differences in collagen I content [32,48], and this may have affected the way in which these materials react to the generation of EngNT. B-ECM hydrogels began to stiffen at much higher strains, and so this likely accounts for their improved structural integrity following contraction and plastic compression.

Cellular hydrogel contraction is a prerequisite for cellular self-alignment in the process of producing EngNT constructs [39]. Contraction assays showed a similar dependency on hydrogel and cell concentrations to those observed in collagen I hydrogels by

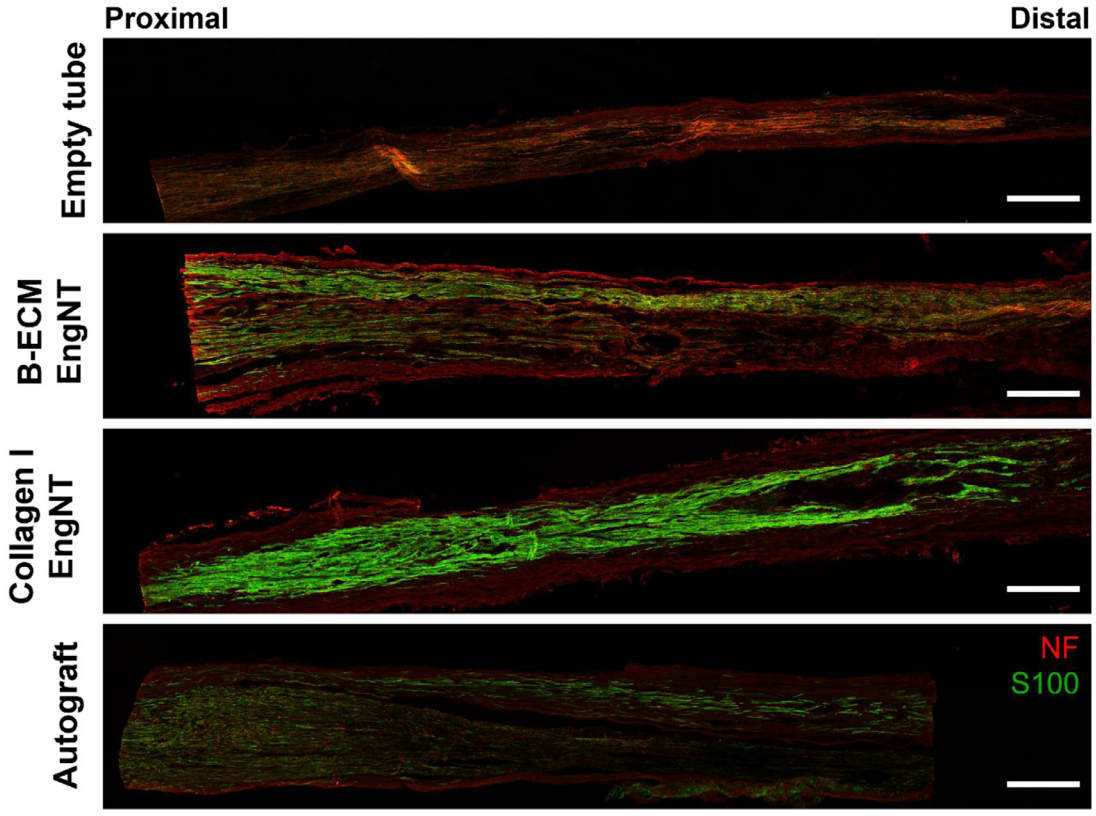

Fig. 5. Neurofilament positive axons and S100 positive Schwann cells within the implanted grafts. Representative confocal micrographs of NF and S100 staining of 6 mm longitudinal sections of autograft, B-ECM EngNT, collagen I EngNT, and empty tube groups 28 days post-surgery. Scale bar = 500 µm.

O'Rourke, Drake, Cameron, Loughlin and Phillips [39]. Moreover, through the CD49α inhibition assay, the magnitude of dECM hydrogel contraction was found to be largely dependent on cell-collagen interactions involving $\boldsymbol{\alpha}1$ integrin. Contraction did not necessarily directly correlate with the self-alignment of the F7 Schwann cells; SIS-ECM and LIV-ECM hydrogels showed similar degrees of contraction at 4×10^6 cells/ml and 4 mg/ml hydrogel concentrations, however, F7 Schwann cells seeded in LIV-ECM hydrogels did not align. On the other hand, F7 Schwann cells within the B-ECM and SIS-ECM hydrogels displayed high levels of cellular alignment. A feature which might contribute to the success of Schwann cell implantation is the influence the biomaterial has on encouraging a repair Schwann cell phenotype [49]. In line with previous work [39,50], greater magnitudes of cellular alignment, and subsequent tissue anisotropy, were associated with an elongated, bipolar F7 Schwann cell morphologies; a hallmark of the repair Schwann cell phenotype [49].

Improving neurite extension is a multifaceted challenge; the extracellular and cellular components of substrates can affect the speed and directionality of extending neurites. For example, some sGAG have been reported to increase neurite extension [51], whilst others are inhibitory [52,53]. Structural ECM components can affect neurite extension: laminin increases neurite extension [54–56], whilst there are conflicting reports with collagen I [55–57]. It was therefore surprising that coating coverslips with dECM showed that the biochemical profiles of the dECM appeared to have little direct effect on elongation of neurites. On the other hand, the interactions between the cellular dECM EngNT and neurites seems crucial. It is possible to attribute the reduced growth of the neurites on the LIV-ECM EngNT to the lack of cellular alignment as there is consensus that aligned substrates consistently result in increased *in vitro* neurite extension [51,58]. Higher neurite extension on the B-ECM EngNT may further be explained by the mechanical properties of the B-ECM hydrogel. It was shown to have a higher complex modulus, even more so through its strain stiffening response, and so it is likely the structural integrity of the artificial tissue was maintained and a more robust substrate for neurite extension provided. The lower neurite extension on the SIS-ECM EngNT may be due to lower cell viability of the F7 Schwann cells within SIS-ECM hydrogels, thus affecting the neurite extension as shown in Georgiou, Bunting, Davies, Loughlin, Golding and Phillips [12]. Aligned, robust EngNT is therefore likely necessary for providing a substrate that is supportive of neurite extension. The results from these *in vitro* models led to the selection of the 4 mg/ml B-ECM hydrogel for further investigation within an *in vivo* rat injury model.

A 10-mm sciatic defect was repaired using silicone tubes containing either B-ECM derived EngNT and collagen I derived EngNT. Our model used empty silicone tubes and autografts to provide a "floor" and a "ceiling" of regeneration respectively, and was based on previous data published by our group [59]. Central to improving functional outcomes following peripheral nerve injury is preventing chronic denervation via increasing the rate at which axons extend through NGCs or grafts [60]. Axon counts were therefore taken at the distal region of the implanted grafts and controls and compared to the axon counts within the proximal region to assess how the rate of regeneration differs between the groups. The key finding from this experiment was that B-ECM EngNT is as supportive of nerve regeneration as collagen I derived EngNT. Although the autograft group was superior in terms of axonal regeneration, this was in line with previous work by Muangsanit, Roberton, Costa and Phillips [50] where the experimental groups lie within a spectrum of axonal regeneration provided by the empty conduit and autograft groups at either margin. By increasing the time point

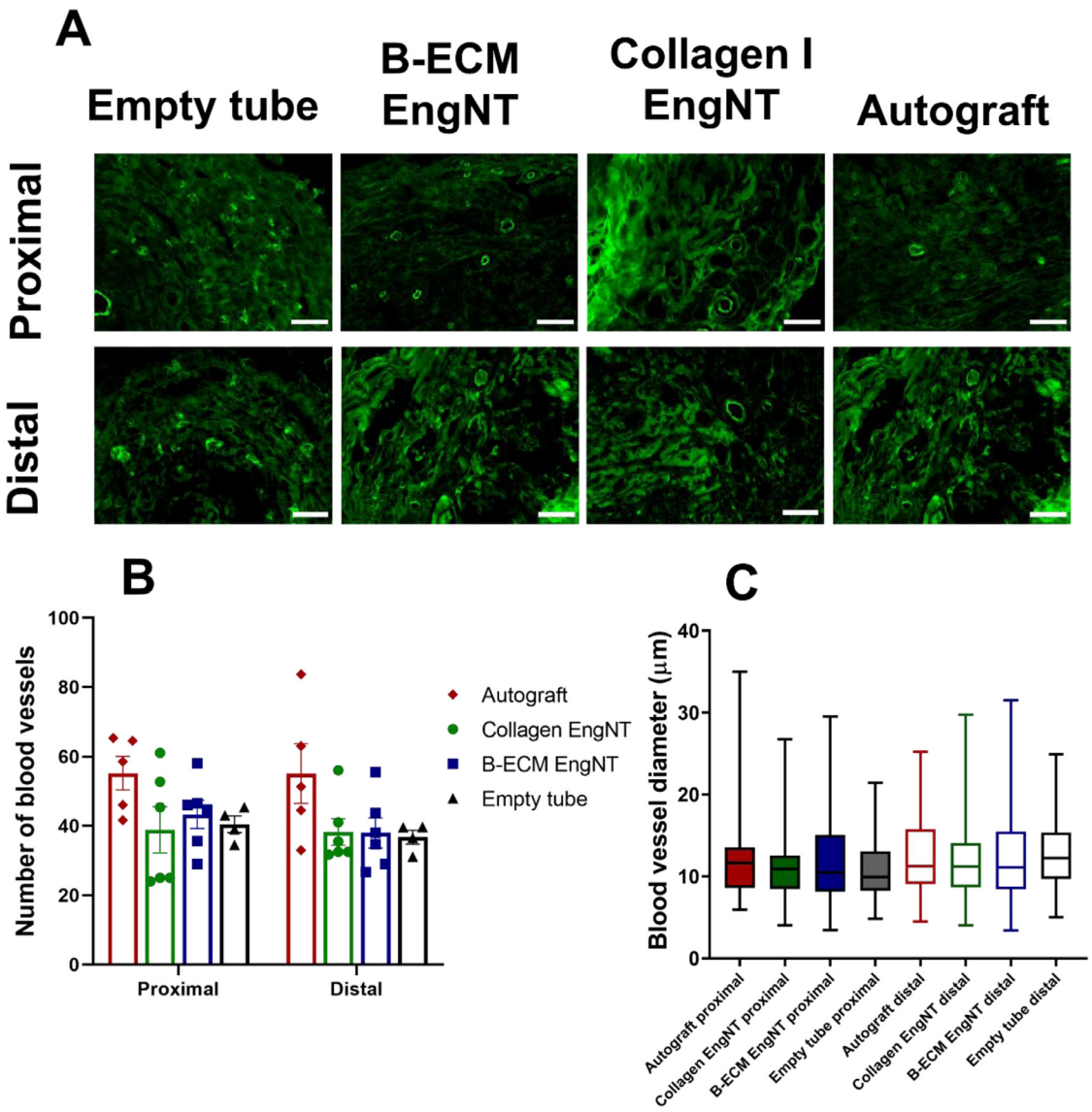

Fig. 6. Vascularisation of B-ECM EngNT is similar to that of collagen I EngNT. Representative fluorescence micrographs of RECA-1 positive blood vessels within the proximal and distal regions of empty tubes, collagen I EngNT, B-ECM EngNT, and autografts 28 days post-surgery. Scale bars = 100 μm [A]. Quantification of RECA-1 positive blood vessels at the proximal and distal regions of each group [B]. Blood vessel diameter [C]. Box plots show min, max, and median with lower and upper quartile. Data are presented as mean ± SEM. n = 6 animals for the B-ECM and collagen EngNT, n=5 animals for the autograft, and n = 4 animals for the empty tube.

of the model, regeneration within the EngNT groups may match that observed in the autograft group. Moreover, due to the limitations in size of the EngNT sheets, the majority of space within the experimental conduits is unoccupied. Therefore, regeneration may be improved by the employment of multiple sheets of EngNT per construct, providing a more robust bridging tissue that could be a more supportive substrate for axonal regeneration. Within these studies a larger gap should be employed, as well as functional tests such as electrophysiological assessments, to gain further insight into how these materials may be aiding the regeneration process.

5. Conclusion

In summation, dECM hydrogels were diverse in biochemical composition and thus, different cellular responses to each dECM was observed. The results from this study have shown, for the first time, that hydrogels derived from xenogeneic non-tissue specific tissues, when incorporated into EngNT, can promote neurite extension *in vitro* as well as axonal regeneration *in vivo*. This study therefore sets a precedent for further investigating the utilisation of more sophisticated biomaterials, such as dECMh, to be incorporated into EngNT for peripheral nerve repair.

Declaration of Competing Interest

The authors declare that they have no known competing financial interests or personal relationships that could have appeared to influence the work reported in this paper.

Supplementary materials

Supplementary material associated with this article can be found, in the online version, at doi:10.1016/j.actbio.2022.12.003.

References

[1] W.Z. Ray, S.E. Mackinnon, Management of nerve gaps: autografts, allografts, nerve transfers, and end-to-side neurorrhaphy, Exp. Neurol. 223 (1) (2010) 77–85.

[2] F. Lassner, M. Becker, A. Berger, Degeneration and regeneration in nerve autografts and allografts, Microsurgery 16 (1) (1995) 4–8.
[3] C.R. Carvalho, J.M. Oliveira, R.L. Reis, Modern trends for peripheral nerve repair and regeneration: beyond the hollow nerve guidance conduit, Front. Bioeng. Biotechnol. 7 (2019) 337.
[4] S. Kehoe, X.F. Zhang, D. Boyd, FDA approved guidance conduits and wraps for peripheral nerve injury: a review of materials and efficacy, Injury 43 (5) (2012) 553–572.
[5] P. Konofaos, J.P. Ver Halen, Nerve repair by means of tubulization: past, present, future, J. Reconstr. Microsurg. 29 (3) (2013) 149–163.
[6] M.S. Arda, E.A. Koçman, E. Özkara, E. Söztutar, O. Özatik, A. Köse, C. Çetin, Can a small intestine segment be an alternative biological conduit for peripheral nerve regeneration? Balkan Med. J. 34 (3) (2017) 246–254.
[7] Y. Wang, H. Jia, W.Y. Li, X.J. Tong, G.B. Liu, S.W. Kang, Synergistic effects of bone mesenchymal stem cells and chondroitinase ABC on nerve regeneration after acellular nerve allograft in rats, Cell. Mol. Neurobiol. 32 (3) (2012) 361–371.
[8] M.L.D. Rayner, A.G.E. Day, K.S. Bhangra, J. Sinden, J.B. Phillips, Engineered neural tissue made using clinical-grade human neural stem cells supports regeneration in a long gap peripheral nerve injury model, Acta Biomater. (2021).
[9] M. Georgiou, S.C.J. Bunting, H.A. Davies, A.J. Loughlin, J.P. Golding, J.B. Phillips, Engineered neural tissue for peripheral nerve repair, Biomaterials 34 (30) (2013) 7335–7343.
[10] M. Georgiou, J.P. Golding, A.J. Loughlin, P.J. Kingham, J.B. Phillips, Engineered neural tissue with aligned, differentiated adipose-derived stem cells promotes peripheral nerve regeneration across a critical sized defect in rat sciatic nerve, Biomaterials 37 (2015) 242–251.
[11] C. O'Rourke, A.G.E. Day, C. Murray-Dunning, L. Thanabalasundaram, J. Cowan, L. Stevanato, N. Grace, G. Cameron, R.A.L. Drake, J. Sinden, J.B. Phillips, An allogeneic 'off the shelf' therapeutic strategy for peripheral nerve tissue engineering using clinical grade human neural stem cells, Sci. Rep. 8 (1) (2018) 2951-2951.
[12] M. Georgiou, S.C. Bunting, H.A. Davies, A.J. Loughlin, J.P. Golding, J.B. Phillips, Engineered neural tissue for peripheral nerve repair, Biomaterials 34 (30) (2013) 7335–7343.
[13] M.L.D. Rayner, A.G.E. Day, K.S. Bhangra, J. Sinden, J.B. Phillips, Engineered neural tissue made using clinical-grade human neural stem cells supports regeneration in a long gap peripheral nerve injury model, Acta Biomater. 135 (2021) 203–213.
[14] L.T. Saldin, M.C. Cramer, S.S. Velankar, L.J. White, S.F. Badylak, Extracellular matrix hydrogels from decellularized tissues: structure and function, Acta Biomater. 49 (2017) 1–15.
[15] Y. Wu, J. Wang, Y. Shi, H. Pu, R.K. Leak, A.K.F. Liou, S.F. Badylak, Z. Liu, J. Zhang, J. Chen, L. Chen, Implantation of brain-derived extracellular matrix enhances neurological recovery after traumatic brain injury, Cell Transplant. 26 (7) (2017) 1224–1234.
[16] D. Tukmachev, S. Forostyak, Z. Koci, K. Zaviskova, I. Vackova, K. Vyborny, I. Sandvig, A. Sandvig, C.J. Medberry, S.F. Badylak, E. Sykova, S. Kubinova, Injectable extracellular matrix hydrogels as scaffolds for spinal cord injury repair, Tissue Eng. Part A 22 (3-4) (2016) 306–317.
[17] Z. Kočí, K. Výborný, J. Dubišová, I. Vacková, A. Jäger, O. Lunov, K. Jiráková, Š. Kubinová, Extracellular matrix hydrogel derived from human umbilical cord as a scaffold for neural tissue repair and its comparison with extracellular matrix from porcine tissues, Tissue Eng. Part C: Methods 23 (6) (2017) 333–345.
[18] R.C. Cornelison, E. Gonzalez-Rothi, S.L. Porvasnik, S.M. Wellman, J.H. Park, D.D. Fuller, C.E. Schmidt, Injectable hydrogels of optimized acellular nerve for injection in the injured spinal cord, Biomed. Mater. (2018).
[19] X. Zhou, J. Wang, X. Huang, W. Fang, Y. Tao, T. Zhao, C. Liang, J. Hua, Q. Chen, F. Li, Injectable decellularized nucleus pulposus-based cell delivery system for differentiation of adipose-derived stem cells and nucleus pulposus regeneration, Acta Biomater. 81 (2018) 115–128.
[20] N. Rao, G. Agmon, M.T. Tierney, J.L. Ungerleider, R.L. Braden, A. Sacco, K.L. Christman, Engineering an injectable muscle-specific microenvironment for improved cell delivery using a nanofibrous extracellular matrix hydrogel, ACS Nano 11 (4) (2017) 3851–3859.
[21] C. Damian, H. Ghuman, C. Mauney, R. Azar, J. Reinartz, S.F. Badylak, M. Modo, Post-stroke timing of ECM hydrogel implantation affects biodegradation and tissue restoration, Int. J. Mol. Sci. 22 (21) (2021).
[22] M. Modo, H. Ghuman, R. Azar, R. Krafty, S.F. Badylak, T.K. Hitchens, Mapping the acute time course of immune cell infiltration into an ECM hydrogel in a rat model of stroke using (19)F MRI, Biomaterials 282 (2022) 121386.
[23] H.L. Xu, F.R. Tian, J. Xiao, P.P. Chen, J. Xu, Z.L. Fan, J.J. Yang, C.T. Lu, Y.Z. Zhao, Sustained-release of FGF-2 from a hybrid hydrogel of heparin-poloxamer and decellular matrix promotes the neuroprotective effects of proteins after spinal injury, Int. J. Nanomed. 13 (2018) 681–694.
[24] C. Zheng, Z. Yang, S. Chen, F. Zhang, Z. Rao, C. Zhao, D. Quan, Y. Bai, J. Shen, Nanofibrous nerve guidance conduits decorated with decellularized matrix hydrogel facilitate peripheral nerve injury repair, Theranostics 11 (6) (2021) 2917–2931.
[25] Z. Rao, T. Lin, S. Qiu, J. Zhou, S. Liu, S. Chen, T. Wang, X. Liu, Q. Zhu, Y. Bai, D. Quan, Decellularized nerve matrix hydrogel scaffolds with longitudinally oriented and size-tunable microchannels for peripheral nerve regeneration, Mater. Sci. Eng. C Mater. Biol. Appl. 120 (2021) 111791.
[26] S. Qiu, Z. Rao, F. He, T. Wang, Y. Xu, Z. Du, Z. Yao, T. Lin, L. Yan, D. Quan, Q. Zhu, X. Liu, Decellularized nerve matrix hydrogel and glial-derived neurotrophic factor modifications assisted nerve repair with decellularized nerve matrix scaffolds, J. Tissue Eng. Regen. Med. 14 (7) (2020) 931–943.
[27] R. Li, J. Xu, Z. Rao, R. Deng, Y. Xu, S. Qiu, H. Long, Q. Zhu, X. Liu, Y. Bai, D. Quan, Facilitate angiogenesis and neurogenesis by growth factors integrated decellularized matrix hydrogel, Tissue Eng. Part A (2020).
[28] S. Ozbek, P.G. Balasubramanian, R. Chiquet-Ehrismann, R.P. Tucker, J.C. Adams, The evolution of extracellular matrix, Mol. Biol. Cell 21 (24) (2010) 4300–4305.
[29] T. Lin, S. Liu, S. Chen, S. Qiu, Z. Rao, J. Liu, S. Zhu, L. Yan, H. Mao, Q. Zhu, D. Quan, X. Liu, Hydrogel derived from porcine decellularized nerve tissue as a promising biomaterial for repairing peripheral nerve defects, Acta Biomater. 73 (2018) 326–338.
[30] T.A. Prest, E. Yeager, S.T. LoPresti, E. Zygelyte, M.J. Martin, L. Dong, A. Gibson, O.O. Olutoye, B.N. Brown, J. Cheetham, Nerve-specific, xenogeneic extracellular matrix hydrogel promotes recovery following peripheral nerve injury, J. Biomed. Mater. Res. Part A (2017) 450–459.
[31] C. Gentili/snm, R. Cancedda, Cartilage and bone extracellular matrix, Curr. Pharm. Des. 15 (12) (2009) 1334–1348.
[32] M.J. Sawkins, W. Bowen, P. Dhadda, H. Markides, L.E. Sidney, A.J. Taylor, F.R.A.J. Rose, S.F. Badylak, K.M. Shakesheff, L.J. White, Hydrogels derived from demineralized and decellularized bone extracellular matrix, Acta Biomater. 9 (8) (2013) 7865–7873.
[33] B. Wildemann, A. Kadow-Romacker, N.P. Haas, G. Schmidmaier, Quantification of various growth factors in different demineralized bone matrix preparations, J. Biomed. Mater. Res. Part A 81A (2) (2007) 437–442.
[34] R.M. Smith, C. Wiedl, P. Chubb, C.H. Greene, Role of Small Intestine Submucosa (SIS) as a nerve conduit: preliminary report, J. Invest. Surg. 17 (6) (2004) 339–344.
[35] R. Zhukauskas, D.N. Fischer, C. Deister, N.Z. Alsmadi, D. Mercer, A comparative study of porcine small intestine submucosa and cross-linked bovine type I collagen as a nerve conduit, J. Hand Surg. Glob. Online 3 (5) (2021) 282–288.
[36] K. Schenke-Layland, O. Vasilevski, F. Opitz, K. König, I. Riemann, K.J. Halbhuber, T. Wahlers, U.A. Stock, Impact of decellularization of xenogeneic tissue on extracellular matrix integrity for tissue engineering of heart valves, J. Struct. Biol. 143 (3) (2003) 201–208.
[37] A.E. Loneker, D.M. Faulk, G.S. Hussey, A. D'Amore, S.F. Badylak, Solubilized liver extracellular matrix maintains primary rat hepatocyte phenotype in-vitro, J. Biomed. Mater. Res. - Part A 104 (4) (2016) 957–965.
[38] S.F. Badylak, B. Kropp, T. McPherson, H. Liang, P.W. Snyder, Small intestional submucosa: a rapidly resorbed bioscaffold for augmentation cystoplasty in a dog model, Tissue Eng. 4 (4) (1998) 379–387.
[39] C. O'Rourke, R.A.L. Drake, G.W.W. Cameron, A.J. Loughlin, J.B. Phillips, Optimising contraction and alignment of cellular collagen hydrogels to achieve reliable and consistent engineered anisotropic tissue, J. Biomater. Appl. 30 (5) (2015) 599–607.
[40] T.W. Gilbert, J. Freund, S.F. Badylak, Quantification of DNA in biologic scaffold materials, J. Surg. Res. 152 (1) (2009) 135–139.
[41] J.B. Phillips, R. Brown, Micro-structured materials and mechanical cues in 3D collagen gels, Methods Mol. Biol. 695 (2011) 183–196.
[42] M.J. Buckenmeyer, T.J. Meder, T.A. Prest, B.N. Brown, Decellularization techniques and their applications for the repair and regeneration of the nervous system, Methods 171 (March 2019) (2020) 41–61.
[43] R. Londono, J.L. Dziki, E. Haljasmaa, N.J. Turner, C.A. Leifer, S.F. Badylak, The effect of cell debris within biologic scaffolds upon the macrophage response, J. Biomed. Mater. Res. - Part A 105 (8) (2017) 2109–2118.
[44] F.E. Uhl, F. Zhang, R.A. Pouliot, J.J. Uriarte, S. Rolandsson Enes, X. Han, Y. Ouyang, K. Xia, G. Westergren-Thorsson, A. Malmstrom, O. Hallgren, R.J. Linhardt, D.J. Weiss, Functional role of glycosaminoglycans in decellularized lung extracellular matrix, Acta Biomater. 102 (2020) 231–246.
[45] U. Mendibil, R. Ruiz-Hernandez, S. Retegi-Carrion, N. Garcia-Urquia, B. Olalde–Graells, A. Abarrategi, Tissue-specific decellularization methods: rationale and strategies to achieve regenerative compounds, Int. J. Mol. Sci. 21 (15) (2020).
[46] O. Syed, N.J. Walters, R.M. Day, H.W. Kim, J.C. Knowles, Evaluation of decellularization protocols for production of tubular small intestine submucosa scaffolds for use in oesophageal tissue engineering, Acta Biomater. 10 (12) (2014) 5043–5054.
[47] L.J. White, A.J. Taylor, D.M. Faulk, T.J. Keane, L.T. Saldin, J.E. Reing, I.T. Swinehart, N.J. Turner, B.D. Ratner, F. Stephen, The impact of detergents on the tissue decellularization process: a ToF-SIMS study, Acta Biomater. 50 (2017) 207–219.
[48] S. Motte, L.J. Kaufman, Strain stiffening in collagen I networks, Biopolymers 99 (1) (2013) 35–46.
[49] K.R. Jessen, R. Mirsky, The repair Schwann cell and its function in regenerating nerves, J. Physiol. 594 (13) (2016) 3521–3531.
[50] P. Muangsanit, V. Roberton, E. Costa, J.B. Phillips, Engineered aligned endothelial cell structures in tethered collagen hydrogels promote peripheral nerve regeneration, Acta Biomater. (2021).
[51] R. Menezes, S. Hashemi, R. Vincent, G. Collins, J. Meyer, M. Foston, T.L. Arinzeh, Investigation of glycosaminoglycan mimetic scaffolds for neurite growth, Acta Biomater. 90 (2019) 169–178.
[52] D.P. Kuffler, I.J. Sosa, O. Reyes, Schwann cell chondroitin sulfate proteoglycan inhibits dorsal root ganglion neuron neurite outgrowth and substrate specificity via a soma and not a growth cone mechanism, J. Neurosci. Res. 87 (13) (2009) 2863–2871.
[53] J. Zuo, D. Neubauer, J. Graham, C.A. Krekoski, T.A. Ferguson, D. Muir, Regeneration of axons after nerve transection repair is enhanced by degradation of chondroitin sulfate proteoglycan, Exp. Neurol. 176 (1) (2002) 221–228.
[54] S.B. Bailey, M.E. Eichler, A. Villadiego, K.M. Rich, The influence of fibronectin and laminin during Schwann cell migration and peripheral nerve regeneration through silicon chambers, J. Neurocytol. 184 (1993) 176–184.

[55] C. Deister, S. Aljabari, C.E. Schmidt, Effects of collagen 1, fibronectin, laminin and hyaluronic acid concentration in multi-component gels on neurite extension, J. Biomater. Sci. Polym. Ed. 18 (8) (2007) 983–997.
[56] N.E. Zander, J.A. Orlicki, A.M. Rawlett, T.P. Beebe Jr., Surface-modified nanofibrous biomaterial bridge for the enhancement and control of neurite outgrowth, Biointerphases 5 (4) (2010) 149–158.
[57] N.G. Carri, K. Rubin, D. Gullberg, T. Ebendal, Neuritogenesis on collagen substrates. Involvement of integrin-like matrix receptors in retinal fibre outgrowth on collagen, Int. J. Dev. Neurosci. 10 (5) (1992) 393–405.
[58] S. Yao, X. Liu, S. Yu, X. Wang, S. Zhang, Q. Wu, X. Sun, H. Mao, Co-effects of matrix low elasticity and aligned topography on stem cell neurogenic differentiation and rapid neurite outgrowth, Nanoscale 8 (19) (2016) 10252–10265.
[59] P. Muangsanit, A. Day, S. Dimiou, A.F. Atac, C. Kayal, H. Park, S.N. Nazhat, J.B. Phillips, Rapidly formed stable and aligned dense collagen gels seeded with Schwann cells support peripheral nerve regeneration, J. Neural Eng. 17 (4) (2020) 046036.
[60] B.J. Pfister, T. Gordon, J.R. Loverde, A.S. Kochar, S.E. Mackinnon, D.K. Cullen, Biomedical engineering strategies for peripheral nerve repair: surgical applications, state of the art, and future challenges, Crit. Rev. Biomed. Eng. 39 (2) (2011) 81–124.